(61)

Determining the Position of

Underwater Tethers in Real Time

by

Matthew E. Esch

Submitted to the Department of Electrical Engineering and Computer Science

in Partial Fulfillment of the Requirements for the Degrees of

Bachelor of Science in Electrical Science and Engineering

and Master of Engineering in Electrical Engineering and Computer Science

at the Massachusetts Institute of Technology

May 27, 1998

[June 1998]

Author_____
Department of Electrical Engineering and Computer Science
May 27, 1998

Certified by_____
Nathaniel I. Durlach
Senior Research Scientist
Thesis Supervisor

Accepted by_____
Arthur C. Smith
Chairman, Department Committee on Graduate Theses

Determining the Position of
Underwater Tethers in Real Time

by
Matthew E. Esch

Submitted to the
Department of Electrical Engineering and Computer Science

May 27, 1998

In Partial Fulfillment of the Requirements for the Degree of
Bachelor of Science in Electrical Science and Engineering and
Master of Engineering in Electrical Engineering and Computer Science

ABSTRACT

The purpose of this thesis is to present two ways of determining the position of underwater tethers, mathematical tether modeling and sensor system measurement. Though the ideal solution may be a combination of both modeling and measurements, this thesis only covers modeling and measurements individually. The tether model is designed to be placed in a virtual environment (VE) simulator in order help train ROV pilots on tether awareness. The model assumes that the tether will follow the equation of a scaled and shifted catenary. The solution can be found in three dimensions within roughly 4n operations, where n is the number of tether segments making up the catenary. The sensor measurement system uses strain gauges to measure the bending and torsional strains in the tether in order to obtain the position of the tether underwater.

Thesis Supervisor: Nathaniel I. Durlach
Title: Senior Research Scientist

Acknowledgments

I would like to first thank my thesis supervisor for his unending support and guidance. I have never witnessed an advisor who cares more about supplying help to those around him than Nat. The relaxed atmosphere and liberal intellectual freedom he has given me as a graduate student has made my fifth year exciting and rewarding.

I would also like to thank my second advisor, Tom Wiegand, for all of his ideas and inspiration. Almost all of the good ideas presented in this thesis came from him.

I cannot forget all of my friends, both from home and at school, who have always provided entertainment when I needed a break and encouragement when I felt that I could not succeed.

Most importantly, I would like to thank my family for all of the support and love through out my entire life. I owe all that I have to them.

Contents

List of Figures

Chapter 2

Chapter 3

Appendix

1.0 Introduction

Determining the position of deployed tethers is of great importance in many scientific applications. NASA scientists are currently attempting to use tethers for a variety of space applications, such as power generation for satellites and "elevator-like" earth-to-space transportation. Underwater tether applications are even more common including towed measurement systems, underwater cable deployment, and tethered underwater remotely operated vehicles (ROV). The research in this paper will be mostly concerned with the use of underwater tethers in ROV operations. However, the results of this project will certainly pertain to any operation where the position of a deployed cable or tether is needed.

One of the main problems in the use of tethered underwater vehicles is the entanglement of the tether with itself and other objects in the area it is exploring. Currently, the ROV pilot has to create a mental model of the position and shape of the tether given its length, the ROV's position, the vehicle's path in time, the direction and magnitude of the current, and the buoyancy of the tether. Along with everything else that the pilot has to keep track of, this can be a very difficult task. A simple display of the location of the tether would be a tremendous aid.

There are two applications of this display that would be most useful, a performance aid for ROV pilots in the field and an educational tool to help train ROV pilots in a virtual environment (VE) simulator. Each application has its own requirements and appropriate solutions. Section 1.1 discusses the creation of a tether model to be placed in a VE trainer. Section 1.2 presents the need for a measurement system in order to make an accurate performance aid. Section 1.3 provides the layout of the rest of the research.

1.1 Virtual Environment Simulators

The purpose of creating a VE simulator would be to place an ROV pilot into several simulated situations where the awareness of the tether is needed. Each situation could have its own performance criteria and set of goals. For instance, one goal may be to teach a pilot to return along the same path that he/she came from. This practice avoids the problem of wrapping the tether around an obstacle. Another goal may be to keep the pilot from letting out too much tether so that there is a smaller chance of the tether getting caught.

In order to implement any of these goals a model of the tether in open water is needed. The largest concern in selecting a model will be its computation time since this is directly related to its cost of implementation. If a tether model requires many operations to compute a solution, then it will require a very fast and expensive computer for it to run in real time. This cost constraint requires some trade-off between the complexity and accuracy of the model for its speed of computation.

In the VE simulator there will be considerable room to exchange accuracy for speed. As long as the overall goals of the training are kept in mind, the exact location of the tether will not matter. Though the amount of accuracy that can be sacrificed will depend upon the type of mission, in most cases the room for error is quite large.

1.2 Performance Aids

The first attempt at creating a performance aid is through the use of the physical modeling techniques described in Section 1.1. The main advantage of using physical models to determine the position of an underwater tether is its ease of implementation. Once the model is developed and encoded it is quite easy,

outside of cost constraints, to supply a processor to run the model and a monitor to display the tether's position.

However, there are many limitations in using only a tether model to create a performance aid. In order to create this aid for pilots in the field, it would be necessary to accurately model a real tether in the water. A real deployed tether can have many "kinks" and twists due to the very high spatial frequencies along its length. For instance, actual tethers may have significant bending biases, primarily due to drum storage. Tethers can also experience creep as well, meaning that the bending bias is a function of both loading and time. These biases, which are very difficult to model, help determine the real configuration of the tether and need to be included if a real tether is to be modeled. No existing physical model incorporates any of the higher order effects of bending biases or creep [1]. Even if a system did try to model these higher order effects, the environment could always introduce some unexpected results that the model could not take into account.

Using sensors to take measurements along the cable is a way to alleviate this problem. As long as the tether's shape was within certain limits, a sensor system could be designed to measure it directly. Since there would be few assumptions used, a sensor system could obtain accurate results given nearly any situation.

However, there are concerns of relying entirely on a measurement system. The accuracy of the system is directly related to the density of the sensors, the quality of the sensors, and therefore the cost of the sensor system. In order to obtain reasonably accurate results using sensors alone, a very expensive system would be needed. Since cost is always an issue, this option by itself may not be the best alternative.

The ideal solution may be to incorporate both modeling and measurements

into a combined information system. This system would use some key measurements along the tether's length and input these into a simple, physical model. In this system, many of the higher order and unexpected effects of the environment could be included without greatly increasing the cost. However, due to the lack of time, this thesis covers the model and sensor systems individually but, not together.

1.3 Thesis Scope

Chapter 2 presents a number of tether models, each with its own set of assumptions on the environment that the tether is placed in. These assumptions will lead to particular computation time and level of accuracy based on the actual conditions of the environment.

Chapter 3 presents the design for a sensor measurement system composed of strain gauges placed along the length of the tether. Many of the advantages and disadvantages of this system will be presented as well as the possibilities of other types of sensor systems.

Chapter 4 discusses the overall conclusions that can be gained from this research.

The Appendix includes the derivations mentioned in Chapter 2.

2.0 Implementation of Mathematical Tether Models

As mentioned in Section 1.1, the greatest use of tether models is in virtual reality simulators used for training ROV pilots. This chapter will discuss the selection and implementation of a mathematical tether model that will be placed in a training simulator. The main goal of this simulator will be to make pilots more aware of tether related issues. Section 2.1 describes the simulation environment, including what inputs are available to our model and what outputs are needed. Sections 2.2 and 2.3 present two ways of modeling the tether in two dimensions, dynamic and static modeling. A static model is one where the tether is assumed to have come to rest. In a dynamic model the tether is allowed to move. Sections 2.4, 2.5, and 2.6 describes the specific efforts to implement a static model of the tether. Section 2.4 presents a process that can extend the two-dimensional models to three dimensions. Section 2.5 introduces a way of approximating some of the higher order effects on the cable due to the bending biases of tether storage. Section 2.6 shows how the forces on the ROV can be calculated due to a stationary tether. Section 2.7 discusses some conclusions made from the modeling portion of this research.

2.1 Description of the Virtual Environment

Before discussing the different types of tether models that could be used, it is important to examine what the virtual environment will look like and what is required of any model that will be placed in it. The simulator we will be using is in three dimensions and has obstacles placed throughout the environment. The current is assumed to be uniform in one direction, though it can change during a given scenario. The effects of the environment on the ROV itself are already well

modeled. What is needed is a good model of how the environment is affecting the tether and how the tether acts upon the ROV.

Any model that we use must meet certain requirements. Namely, it must produce as an output the position of the tether, which may consist of a number of connected links, and the magnitude and direction of the force applied by the tether on the ROV. The simulation environment will provide a wide range of inputs that can be used by our model. These include the tether's endpoints, the direction and magnitude of the current, the direction and magnitude of the ROV's velocity, the length of tether deployed, and certain properties of the tether. The properties of the tether needed by the models we will be examining are the diameter of the tether, its weight or lift underwater, its drag coefficients with the flow of water, its modulus of elasticity, and the bending radius it is stored at.

2.2 Two-Dimensional Dynamic Tether Models

Dynamic tether models include the effects of the movement of the ROV and the tether when finding the tether's current position. This addition makes these models very complex since the velocity of the tether along its length must be found in addition to its position and tension.

These models make very few assumptions about the tether environment. All existing models neglect the effect of bending biases. In addition, they assume that the tether is relatively uniform in diameter and the current effects are well-behaved, having no waves or vortexes. Each model below will also have its own additional assumptions.

The general method of solution for these models is to balance all of the forces acting at discrete points, connected by stiff links, along the cable. The general equations used for these models are derived in a PhD thesis by Bliek [2].

The forces acting on the tether that are included in all of the dynamic models we examined are the weight or buoyancy of the tether, a fluid inertial force, the drag force due to the current flow, and the tension force in the cable. These forces are set equal to the mass of the cable times the acceleration in the different coordinate directions. Each dynamic model may include or neglect additional interactions however, all of the dynamic models mentioned below use the interactions included in Bliek [2]. All of the dynamic models below place the tether in natural coordinates, which means that the coordinate system is centered around each individual segment of tether. This allows for an easy representation of the forces acting on the tether.

All of the models use finite difference schemes to obtain a solution. The variables solved for in these models are the tension in the tether, the magnitude and direction of the velocity of the tether, and the angle between the links at each discrete point.

2.2.1 Ablow and Schecter's High Tension Model [3]

The first dynamic model examined was done by Ablow and Schecter in 1983. This model was mainly used to model the motion of instrumented cables that were towed behind surface ships and submarines. In these situations, the towed vehicles did not move under their own power which lead to significant tension in the cables and the possibility of stretching.

These conditions lead directly to the additional assumptions made in this model. The tension is assumed to be high along the entire length of the cable and should not vanish at any time. This model assumes that stretching should occur in the cable and that the current is relatively high at all times.

Though this model is well designed for high tension problems, it fails to come up with a solution whenever the tension is zero anywhere along the tether

due to a singularity in the solution matrix. This situation can occur with ROV's when the current is low or the tether is close to being neutrally buoyant.

2.2.2 Howell's Low Tension Model [4, 5]

This model tries to compute the position of a tether in low tension, as in many ROV applications. Since the tension is assumed to be low throughout the cable, this model neglects any stretching in the cable, however, it does include a bending stiffness term. When the tension in the cable becomes very low, this bending stiffness term dominates the equation and a solution can be found.

The only problem with this model arises in the time needed to solve the equations. For a tether with 101 nodes and a time step of .025s, this model provided results in roughly three times real time on a Silicon Graphics IRIS 4D. Though the time steps and the number of nodes are conservative, it would be difficult to make an argument for purchasing an SGI workstation solely to determine the tether's position. Since the training simulator must deal with many other operations, this model, though very accurate in most cases, would take too much time to compute a solution.

2.2.3 Hover's Massless Model [2]

This model tries to speed up the computation time associated with most dynamic tether models by assuming that the tether is massless and using a quaternion representation of the coordinate transformations instead of the usual euler's angle representation. This model contains both low and high tension effects on the tether by including both stretching and bending stiffness. Including both high and low tension effects makes this model useful for almost all ROV applications.

Though the massless assumption greatly simplifies the equations it has not

been determined exactly how fast the model runs since, due to a lack of time, it has not been implemented. The accuracy of the massless approximation is also a concern for this model that needs to be examined.

2.2.4 Two-Dimensional Dynamic Model Results

These models have several advantages. Their solutions include transient motions of the tether caused by the ROV's movements that are not included in the static models. Dependent upon the situation this could be a significant difference. Another advantage is that the dynamic models do not have as much error in low currents, if the models can obtain a solution. This allows these models to be used in a much wider variety of situations.

Though these models are very accurate, the time needed to compute their solutions is too great. As mentioned in Sub-Section 2.2.2, in reference to Howell's model, the training simulator needs to keep track of many other operations; it cannot afford to spend much of its time determining the position of the tether. Since some error in tether display is allowed, this constraint in computation time requires the use of static tether models, which can be computed much faster.

2.3 Two-Dimensional Static Tether Models

A static tether model is one where the velocities of the ROV and the tether are assumed to be much less than the current and are neglected in determining the position of the tether. This assumption greatly simplifies the equations governing the tether and allows it to be defined entirely by its position in a coordinate system and the tension along its length. In many cases this assumption is valid, since the ROV velocity is usually quite small compared to the current. In addition, if the ROV is stationary for a period of time, the actual solution should converge

to the solution obtained through the static model.

The greatest amount of inaccuracy, however, is dependent upon the type of operation being simulated. If 1000 meters of tether is deployed, as in some deep ocean missions, and the area that the ROV is operating in is small, then the effects of the movement of the ROV will be minimal. However, if the site of exploration is a small bay and only 50-100 meters of tether is deployed then the velocity of the ROV may begin to have some effects. This should be taken into consideration when planning specific missions and determining appropriate training behaviors.

There are a few other assumptions that our static models will make as well. They will assume that the tether is relatively uniform in diameter and the current effects are well-behaved, no waves or vortexes. Any bending stiffness or stretching of the tether will also be neglected. Though this model will neglect the effect of bending biases for now, this assumption will be discussed further in Section 2.5.

2.3.1 Finite Element Model

The first static model that has been examined was designed by Dana Yoerger, a researcher at Woods Hole Oceanographic Institute. This model uses finite element analysis in order to determine the position of the tether and the tension along its length. The program running this model computes a numerical solution by trying a variety of forces until it finds a set that brings the cable to the desired position. A Nelder-Mead simplex method is used to solve the equations. From a given starting force, the Nelder-Mead simplex method systematically alters the force to move the cable from the starting position corresponding to the starting force toward the desired position.

After the solution has been reached, the solution for the next simulation step is started with the force from the previous step. This saves some computation time since the tether position in the next step should be close to the position in the previous step. This leaves the problem of how to start initially. To do this, the cable is modeled as a stiff rod directly connecting the base point to the vehicle termination point. The tangential and normal forces for this rod are used to start the approximation procedure.

There is mainly one result of this model that is important to note, its computation time. Each solution takes on average about 100 operations for each tether segment that is used to define the entire tether. This results in a long computation time in order to obtain a given level of accuracy. This model is only included as a comparison to the other static models since the static assumptions embodied in it do not lead to very significant decreases in computation time.

2.3.2 Assumed-Equation Model [6,7]

This static model assumes that the tether's shape can be defined by a shifted and scaled version of a simple equation. This assumption greatly decreases the amount of computation since the model only needs to solve for the parameters of a single equation. In this research, three different equations were examined for accuracy and speed of computation - a hyperbolic cosine (catenary), a parabola, and two jointed line segments. If the tangential drag force due to a uniform velocity current flow can be neglected, the catenary equation is the exact solution. The derivation of this statement is found in Appendix A. The parabola and line segment models were chosen in an attempt to lessen the computation time.

In order to eliminate the effects of current in the solution procedure, the two tether endpoints are first rotated into the current. This reference frame defines

the current as going in the negative y-direction. Using the boundary endpoint conditions (Equation 1 and 2) and the length constraint (Equation 3) we have

$$y_0 = f(x_0) \qquad \text{(Equation 1)}$$

$$y_1 = f(x_1) \qquad \text{(Equation 2)}$$

$$s = \int_{x_0}^{x_1} \sqrt{1 + \left(\frac{df(x)}{dx}\right)^2}\, dx \qquad \text{(Equation 3)}$$

where (x_0, y_0) and (x_1, y_1) are the endpoints of the tether, $f(x)$ is the equation of the tether, and s is the length of the tether. The next step is to solve the equations directly, if possible, or by numerical methods. Once the solution is found, a number of points along the tether are selected and rotated back to the original reference frame defined by the direction of current.

Catenary Assumed-Equation Model

If xs and ys are the x and y shifts respectively and A is the scaling term, the form of the catenary equation is

$$f(x) = A\cosh\left(\frac{x - xs}{A}\right) + ys \qquad \text{(Equation 4)}$$

The three governing equations (Equations 1, 2, and 3 above) give

$$y_0 = A\cosh\left(\frac{x_0 - xs}{A}\right) + ys \qquad \text{(Equation 4a)}$$

$$y_1 = A\cosh\left(\frac{x_1 - xs}{A}\right) + ys \qquad \text{(Equation 4b)}$$

Using $\frac{df(x)}{dx} = \sinh(x)$, $1 + \sinh^2(x) = \cosh^2(x)$, and $\int \cosh(x)dx = \sinh(x) + C$ gives

$$s = A\left[\sinh\left(\frac{x_1 - xs}{A}\right) - \sinh\left(\frac{x_0 - xs}{A}\right)\right] \qquad \text{(Equation 4c)}$$

Since one of the parameters of the catenary equation, the scaling term A, is both inside and outside the transcendental function $\sinh(x)$ in Equation 4c, its solution cannot be solved for directly. Some form of numerical solution is needed. We used a minimization procedure to minimize the error until a solution was found.

The comparison of the catenary model and the finite element model described in section 2.2.1 is shown in Figure 1 for a number of given endpoints. It is easy to see that the solutions of the two models are almost identical.

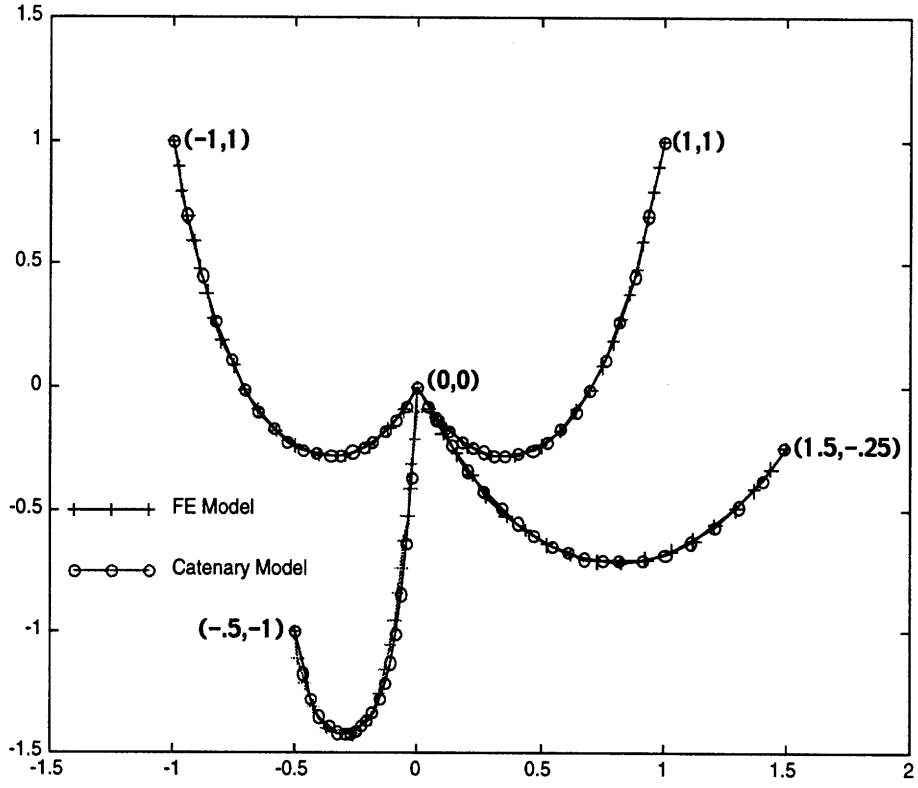

Figure 1. Comparison of Finite Element and Catenary Models

These results make sense. The normal drag coefficient of the tether in the finite element model was 1.5 while the tangential drag coefficient was only 0.003. This vast difference allows us to neglect the tangential drag force, the major assumption of the catenary model. Therefore, whenever the difference in drag coefficients is as great, the catenary model is nearly identical to the finite element model. It should be noted that the values of the coefficients used in the finite element model are typical of most uniform ROV tethers.

Though the general method of solution for the catenary, assumed-equation model is quite fast, improvements can still be made. If the number of tether segments needed for the simulation is low (~10), then coming up with a numerical solution takes up most of the program's computation time. In order to reduce the computation time for a normal numerical solution we tried two common techniques.

The first attempt is an interpolation table. This three-dimensional structure has the solution for the catenary equation given the x and y values of a tether endpoint, assuming the other endpoint is at the origin, and the length of the tether. This table is made once and does not need to be made again while the program is running. The program will search for the nearest points in the table and interpolate a solution. It is about 4x as fast as the regular minimization procedure but, sometimes returns inconsistent results. This happens especially when the two tether endpoints are near each other and there is sufficient slack in the tether. If more solution points are added to the interpolation table near the origin, the number of inconsistent results can be minimized but, not removed entirely.

The other method of reducing the computation time is to use the previous solution as an initial guess for the numerical method. In the normal minimization procedure, a set value is used as the initial guess. Since our model already assumes that the ROV will not move very fast the previous solution should be

very close to the current solution. In our program if we moved the ROV at a maximum of 10% of its distance from the base point, the previous solution method was about 3x as fast. This method is preferred since the speed increase is comparable to the interpolation table and does not introduce any irregularities.

Parabola Assumed-Equation Model

The form of the parabola equations using A, xs, and ys is

$$f(x) = A(x - xs)^2 + ys \qquad \text{(Equation 5)}$$

The three governing equations (Equations 1, 2, and 3 above) give

$$y_0 = A(x_0 - xs)^2 + ys \qquad \text{(Equation 5a)}$$

$$y_1 = A(x_1 - xs)^2 + ys \qquad \text{(Equation 5b)}$$

Using $\int \sqrt{u^2 + a^2}\,du = \frac{u}{2}\sqrt{u^2 + a^2} + \frac{1}{2}\ln\left|u + \sqrt{u^2 + a^2}\right| + C$ and $u = \frac{df(x)}{dx} = 2A(x - xs)$ gives

$$s = \frac{u}{4A}\sqrt{u^2 + 1} + \frac{1}{4A}\ln\left|u + \sqrt{u^2 + 1}\right| \qquad \text{(Equation 5c)}$$

Like the catenary equation, the parabola equation cannot be solved for directly. This makes the parabola model just as slow as the catenary model. Since the catenary is the exact solution and the parabola was only to be used as an approximation, the parabola model will not be used. It is presented here only for completeness.

Straight Line Segment Assumed-Equation Model

The form of the line segment equation using A, xs, and ys is

$$f(x) = A|x - xs| + ys \qquad \text{(Equation 6)}$$

The three governing equations (Equations 1, 2, and 3 above) give

$$y_0 = -A(x_0 - xs) + ys \qquad \text{(Equation 6a)}$$

$$y_1 = A(x_1 - xs) + ys \qquad \text{(Equation 6b)}$$

and since $\frac{df(x)}{dx} = \pm A$=constant

$$s = \sqrt{1 + A^2}(x_1 - x_0) \qquad \text{(Equation 6c)}$$

Unlike the previous two models, the line segment model can be solved for directly. Since the solution can be computed in a few simple operations this model is very fast compared to the catenary and parabola models.

Two-Dimensional Assumed Equation Model Results

Figure 2 below shows the results of the three assumed equation models. As can be seen all three models have the same general appearance. The number of operations needed for these two dimensional models is approximately $1n + T_S$, where n is the number of tether segments and T_S is the time for the numerical solution.

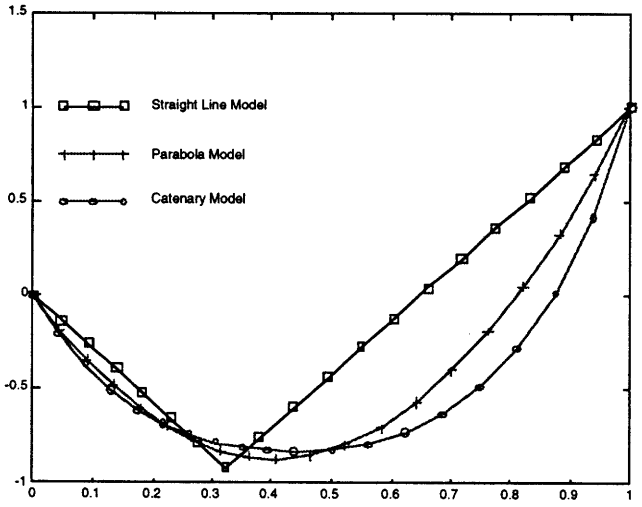

Figure 2. Comparison of 2D Tether Models

The choice of model will depend mainly on the type of mission and training exercise. In some cases, the line segment model may be enough but, in others the catenary would probably be needed. The rest of this chapter will assume that two-dimensional model will be the static catenary assumed equation model.

2.4 Three-Dimensional Static Tether Model

Since the simulation environment and most of the tether problems are in three dimensions, a three-dimensional tether model needs to be designed. This section describes a procedure of converting our two-dimensional assumed equation model into three dimensions. In this way our two-dimensional methods of solution described in Section 2.3 will still be valid.

2.4.1 Neutrally Buoyant Tether

If the tether is neutrally buoyant, it will still be in a two-dimensional plane but, somewhat transformed due to the z-component of the ROV's position. There

are two ways of visualizing this transformation. The first is that the normal vector to the plane that the catenary is in is the cross product of the current flow vector and the ROV's position vector. This can be seen in Figure 3. Another way of visualizing this transformation is by a simple rotation. If the starting point of the tether is at the origin (0,0,0), the plane that the catenary is in can also be obtained by a rotation about the x-y axis or in the x-z plane.

Therefore, the method of solution is to first rotate the tether's endpoints onto the x-y plane and then solve for the two-dimensional catenary solution. Once this is found, the tether segments making up this solution can be rotated back to the catenary plane.

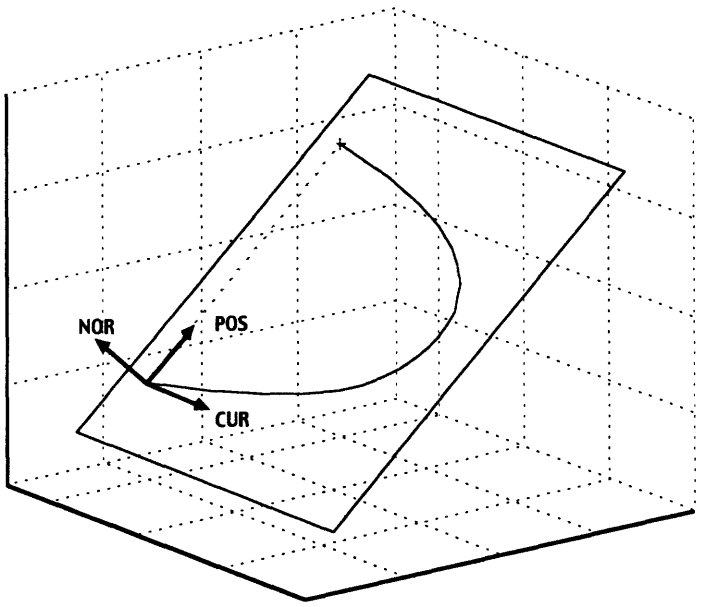

Figure 3. Example of 2D to 3D Conversion for a Neutrally Buoyant Tether

2.4.2 Heavy or Buoyant Tether

If the tether has some amount of weight or lift, the procedure above needs to augmented. Again this procedure can be thought of in two ways. One way is to alter the current vector by the weight force F_W. This is a little difficult since

the current vector is a velocity and the weight vector is a force per unit length of tether. However, the magnitude of the drag force per unit length $|F_D|$, acting upon the tether is $|F_D| = K_D|U|^2$, where K_D is a normal drag force coefficient defined by properties of the tether and U is the velocity of the current. This allows the resultant force to be the addition of F_D and F_W. This resultant force would be called the applied force vector. The normal vector of the catenary plane is now the cross product of this new applied force vector and the position vector. As in the neutrally buoyant case, this addition of the weight of the tether can also be thought of as a new rotation, this time about the x-axis or in the y-z plane.

2.4.3 Three-Dimensional Static Model Results

The computation cost for the 2D to 3D conversion is very small. It only takes 1 or 2 more operations per segment beyond the two-dimensional model. The overall number of operations is now approximately $(2 \text{ or } 3)n + T_S$, depending on whether or not the tether is neutrally buoyant.

One additional advantage is that the model now comes up with a solution when the magnitude of the current goes to zero. The weight force will then determine the shape of the catenary. Normally, in the two-dimensional case, if the magnitude of the current was zero, there would be no solution. In the no current case our assumption about neglecting the ROV velocity may not be as valid but, at least a solution can be found.

One other comment that needs to be made is that the addition of a weight per unit length of the tether does not exactly equate to a rotation in the y-z plane. The procedure stated in Sub-Section 2.4.2 is only an approximation. The real solution would actually be a combination of two catenaries, one caused by the current, the flow catenary, and another perturbing the flow catenary in the z

direction. However, the effects of this difference are minimal and in the limits of the current going to zero and the weight going to zero, the solutions are the same.

2.5 Bending Biases Model

In this section we will try to add a higher order effect on to our three-dimensional model of the tether, bending biases. As mentioned before, bending biases are introduced in the tether after it has been stored on a drum for a long period of time. When the tether is deployed it will look like a coil. To physically model this phenomenon would be very difficult since the shape can change as a function of both the tension in the tether and time. Following along the lines of the assumed equation model presented in Sub-Section 2.3.2, we will try to approximate the bending bias in the tether as an equation and then examine our results.

2.5.1 Helix Equation

The equation we will use is the constant radius helix. The three-dimensional function is defined by

$$x = R\cos\left(\frac{2\pi}{T}z\right) \qquad \text{(Equation 7a)}$$

$$y = R\sin\left(\frac{2\pi}{T}z\right) \qquad \text{(Equation 7b)}$$

where R is the radius and T is the period of the helix. Figure 4 shows the helix.

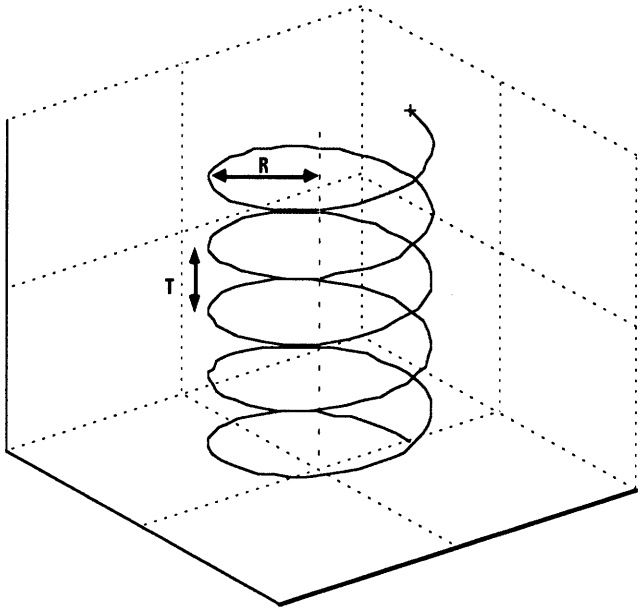

Figure 4. A 3D Helix

Using the length of a curve equation, $s = \int_{x_0}^{x_1} \sqrt{1 + \left(\frac{df(x)}{dx}\right)^2}\, dx$ (Equation 3), we can obtain the length of the helix between any two z coordinates, z_1 and z_0, where $z_1 \geq z_0$ and the height H of the helix is $H = z_1 - z_0$,

$$L = (z_1 - z_0)\sqrt{\left(\frac{2\pi R}{T}\right)^2 + 1} = H\sqrt{\left(\frac{2\pi R}{T}\right)^2 + 1} \qquad \text{(Equation 8)}$$

2.5.2 Helix Model

To complete this model the helix must now be placed along the three-dimensional model of Section 2.4. The result is displayed in Figure 5. The dotted line represents the catenary previously solved for and the swirls around it are due to the helix equation. This solution is obtained by rotating and shifting a piece of the helix to each segment of the catenary model.

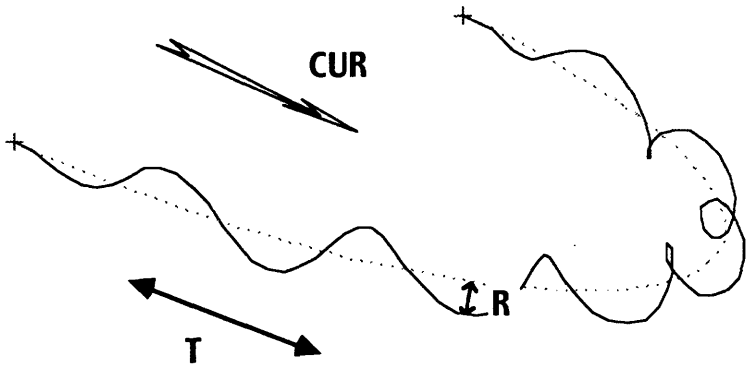

Figure 5. 3D Helix Tether Model

The complexity in this model lies in finding the length of the catenary that the helix will be placed around and the radius, period, and height of the helix. Using Equation 8, with L being the overall length of the tether and h being the height of the helix and the length of the catenary we are solving for we obtain

$$\frac{L}{h} = \sqrt{\left(\frac{2\pi r}{t}\right)^2 + 1} \qquad \text{(Equation 9)}$$

where r is the radius and t is the period of the helix we are solving for. If D is the distance between the two endpoints, at $D = L$ the radius r will go to 0 and at D = 0 the radius r will go to the radius of the drum that the tether is stored on, R_D. By linearly approximating this relationship we obtain the following relation

$$r = -\left(\frac{R_D}{L}\right)D + R_D \qquad \text{(Equation 10)}$$

where both D and L are known as inputs to the model. Now, in Equation 9, we are just left with two unknowns, h and t. Using the same logic in the formulation of Equation 10, we can say that at $D = L$ the period of the helix t will go to

$2\pi R_D$, the circumference of the stored tether. At $D = 0$ the period t will go to zero. Again by linear approximations we obtain

$$t = \frac{2\pi R_D}{L} D \qquad \text{(Equation 11)}$$

By combining Equations 9, 10, and 11 we can obtain an equation for h in terms of L and D, both known values.

$$h = \frac{L}{\sqrt{\left(\frac{L}{D} - 1\right)^2 + 1}} \qquad \text{(Equation 12)}$$

2.5.3 Bending Biases Model Results

The computation cost of adding in bending biases is not very high. For each catenary segment there will be a rotation and a shift of the helix. It may also be necessary to find the magnitude of each catenary segment if they are not all the same length. The amount of operations for the entire solution will be $(5 \text{ or } 6)n + T_S$. Though this figure is low, there may be an additional cost of modeling the bending biases of the tether. If a good visual representation of the tether is desired, many more tether segments will be needed for the bending biases case as opposed to the non-bending biases case. For a normal catenary, 20 segments is more than enough for a good visual representation. With bending biases, 100 or more segments would be required.

The only major questions of accuracy in this model are the linear relationships of radius r and period t of the helix with the distance D of the endpoints. In reality these parameters are probably more linearly related to the tension in the tether but, we feel that this relationship should give good enough results for the simulation.

2.6 Forces Model [8,9]

To determine the forces acting on the ROV in the static case, this section calls on the equations obtained the Appendix A and B, specifically Equations A19 and A26. The constant tension T_D induced in a tether due to a current flow can be solved from the transcendental equation

$$S = \frac{T_D}{K}\sinh\left(\frac{K}{T_D}L\right) \qquad \text{(Equation 13)}$$

where S is the length of the tether from the minimum point to the ROV, K is the overall drag coefficient defined in Appendix A, and L is the span in x-axis from the minimum point to the ROV. The tension T_W induced at the ROV attachment point caused by the tether's weight is

$$T_W = \mu y \qquad \text{(Equation 14)}$$

where μ is the weight per unit length of the tether and y is the span in the y-axis from the minimum point of the tether to the ROV. The total tension in the tether at the ROV attachment point will be the addition of these two tensions. It should be noted that as the weight in the tether goes to zero the tension will be that found in Equation 13 and as the current goes to zero the tension will be that found in Equation 14.

The procedure of solution is very similar to the three-dimensional procedure stated in Section 2.4. First the catenary plane is rotated to the x-y plane. Then the tension at the ROV is found in this two-dimensional reference frame. This is accomplished by using the parameters of the two-dimensional rotated catenary to solve Equations 13 and 14. Just as the segments of the catenary are rotated back

to the catenary plane, so will the tension vectors. These rotated tension vectors will be the forces acting on the ROV.

One might expect that since the position of the tether segments is known that balancing the forces would be a quicker way to solve for the forces acting on the ROV. However, if there is a weight or lift in the tether, the three-dimensional shape of the tether may not be exactly correct, as stated in Sub-Section 2.4.3, and a balance of forces would not result in the correct forces on the ROV.

Essentially, using Equation 13 and Equation 14 finds the tension as if the tether was in the exactly correct position. Since the variable T_D in Equation 13 is on the inside and outside of the transcendental function, the model will need to compute a numerical solution to obtain this tension. An interpolation table could be used to help speed up the computation since it would only be a linear array based on one variable.

2.7 Tether Modeling Results

Overall the Catenary Assumed Equation Model presents a reasonably accurate model of the tether that can be computed very quickly. The approximations are well-founded and lead to a great reduction in computation time compared to the dynamic physical models and the finite element model discussed in Section 2.2 and Sub-Section 2.3.1, respectively.

There are limitations, however, and they have been stated throughout this chapter. The selection of a tether model to use in a simulation should be based on a combination of the type of mission, its training objectives, and the speed of the computer used. In most cases the Catenary Model with the additions described in Sections 2.4, 2.5, and 2.6 should be sufficient. However, if a dynamic analysis is needed to teach a specific type of goal then it would be necessary to implement a

tether model that incorporates the motions of the ROV and purchase a very fast processor. Another possibility in this case is to teach those goals to the pilots in the field and not in simulation.

3.0 Design of Sensor System for Tether Measurement

This chapter describes a possible sensor system using strain gauges to determine the position of the tether. Section 3.1 discusses the background of the strain gauge technology that we plan to use and how these measurements will produce a three-dimensional shape. Section 3.2 discusses the results expected from this application, including the density of sensors needed, their accuracy, and cost. Section 3.3 examines the possibility of alternative technologies. Section 3.4 describes future research that could further develop the work presented in this chapter.

3.1 Strain Gauges [10]

Strain itself is defined as the ratio of the change in length of a material to its initial unstressed length. For any structure there are three types of strain that we will be concerned with, axial, bending, and torsional. These strains will be most easily described in reference to the tether.

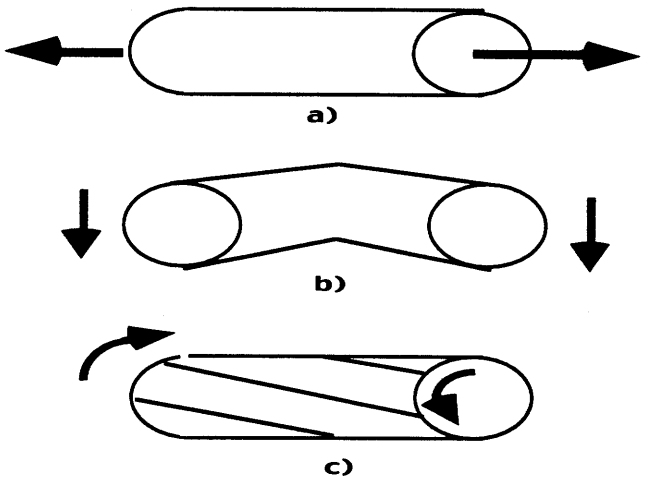

Figure 6. Types of Strain: a) Axial b) Bending c) Rotational

Axial strain is induced when two ends of the tether are pulled apart as

demonstrated in Figure 6a. This change in shape is due to the tension in the tether. Since we do not want this type of strain to enter into our measurements, our positioning of sensors will have to compensate for this. Compensation techniques are discussed later.

Bending strain occurs in the tether when the tether is forced to a particular angle or radius of curvature such as in Figure 6b. The top side of the tether, as shown in the figure, would experience an elongation and the bottom side of the tether would experience a compression. It is this differential in strains that will be measured.

Torsional strain occurs when the tether is twisted about its longitudinal axis, as shown in Figure 6c. Measurements of this type of strain are needed since they will affect how the sensors are orientated in the global coordinate frame.

Strain gauges are able to make these measurements since the electrical resistance of the gauge is proportional to the amount of strain acting on it. This is similar to any wire; when it is stretched its cross sectional area decreases, therefore its resistance increases. In order to measure small amounts of strain and accordingly small changes in resistance, the usual electrical configuration, the Wheatstone Bridge, shown in Figure 7, is used. Note the signs associated with each gauge numbered 1 through 4. The total strain is always the sum of the four strains.

$$\varepsilon_T = \varepsilon_1 - \varepsilon_2 + \varepsilon_3 - \varepsilon_4 \qquad \text{(Equation 15)}$$

The total strain is represented by a change in Vout. If each gauge had the same positive strain, the total would be zero and Vout would remain unchanged, one-half of the regulated DC voltage. If the strain on gauges 1 and 3 is the negative value of the strain on gauges 2 and 4, the total strain would be 4 times

the strain on any one of the gauges. This situation corresponds to a larger output voltage. Therefore the bridge network gives the sensor system greater sensitivity and resolution than using a single strain gauge would.

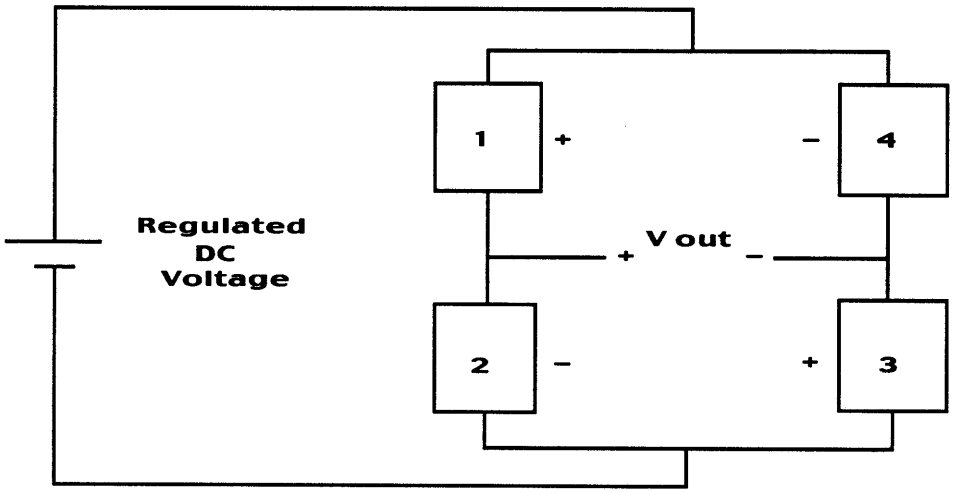

Figure 7. Wheatstone Bridge Network

However, not all four gauges are needed. Due to the small size of the tether and cost constraints, the rest of this chapter will assume that only gauges 1 and 2 will be used, with gauges 3 and 4 being omitted and Vout(-) being tied to ground. The effect of having only two gauges will be dependent on the level of noise in the electrical components connecting the sensors and the amount of sensitivity desired. The amount of electrical noise inherent in the sensor system needs to be found through experimentation and the achievable sensitivity will be discussed more in Section 3.3.

There are several reasons for choosing strain gauges to measure the position of the tether. One reason is because strain gauges can be used for measuring both the bending and twisting of the tether. This is a simple first step since only one type of sensor needs to be understood. At a later stage other possible technologies can be examined and combined to form another sensor system.

A practical advantage of using strain gauges is the low number of electrical lines needed for communication and power. Integrated circuits are available (of Maxim Integrated Products, Inc., MAX 110/MAX 111 and MAX 1246) which incorporate analog to digital conversion with on-chip serially-based communication protocols, allowing the analog outputs of a long line of sensors to be individually selected [11]. Therefore only a few electrical wires are needed to run down the length of the cable; each sensor does not need its own communication line. It may be possible to use other types of sensors in this way but, development of alternative systems would require a significant amount of research.

Though strain gauges are usually used to measure the strain on very stiff pieces of metal, their specifications still meet the requirements of a thin and highly bendable cable. One type of strain gauge, made from etched foil encapsulated in a polyimid film by Omega Engineering, Inc., has a minimum bend radius of .3 mm, a maximum elongation/compression of 5%, and dimension of 10.9 mm by 5.9 mm [10].

The minimum bend radius needed is determined by the radius of the tether. Since most tethers have a radius of at least 1 cm, the specification of .3 mm for the minimum bend radius will be more than enough. The maximum elongation or compression for tethers with copper wire (the limiting factor) is about .5%, a magnitude below the specification for the strain gauges [12]. Since most tethers use copper wire, we will assume that the maximum elongation of .5% is normal for almost all tethers. Since the circumference of a tether with a radius of 1 cm is a little greater than 6 cm, it is feasible to place a few .6 cm strain gauges on its exterior.

3.1.1 Bend Measurements [10, 13]

The layout of the sensors to measure the amount of bending strain is shown in Figure 8. The numbers of the strain gauges, 1 and 2, correspond to their position in the bridge network in Figure 7, omitting strain gauges 3 and 4. The arrangement, as shown in Figure 8, will only measure the bending strain in the vertical plane. Another set of sensors will need to be place on the sides of the tether in order to measure the bending strain in the horizontal plane.

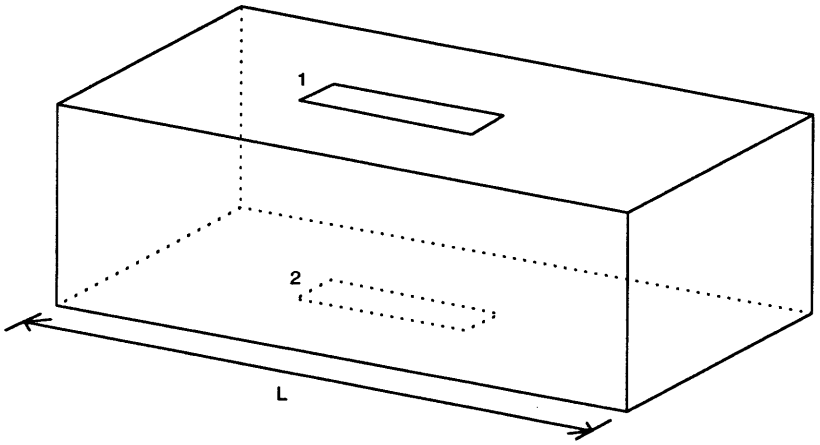

Figure 8. Location of Bend Sensors

If the ends of the structure in Figure 8 are bent downwards, Strain Gauge 1 (SG1) will be elongated and Strain Gauge 2 (SG2) will be compressed. Therefore the resistance of SG1 will decrease and the resistance of SG2 will increase. This will cause an increase in Vout above its normal level, one-half of the regulated voltage. If the ends of the structure are bent upwards, Vout will decrease.

This arrangement also compensates for any axial strain that may be present in the tether. Any axial strain pulling the tether apart will cause both SG1 and SG2 to elongate. Though their resistances will be different than their reference resistance, the resistance of SG1 will equal that of SG2 and Vout will remain at one-half of the regulated voltage.

The next step in finding the position of the tether segment is to use the measurement of bending strain to find the radius of curvature of the tether segment. Consider the tether segment bent around the point A, as shown in Figure 9. The neutral surface is defined as the surface of the material that is not stretched or compressed. The radius of curvature R is the measured distance between the neutral surface and the point A. If θ is the angle in radians between the ends of the tether segment, then the length of the neutral surface l_n is

$$l_n = R\theta \qquad \text{(Equation 16)}$$

if the radius of the tether is y, the length of the elongated surface l_e and the length of the compressed surface l_c are as follows

$$l_e = (R+y)\theta \qquad \text{(Equation 17)}$$

and

$$l_c = (R-y)\theta \qquad \text{(Equation 18)}$$

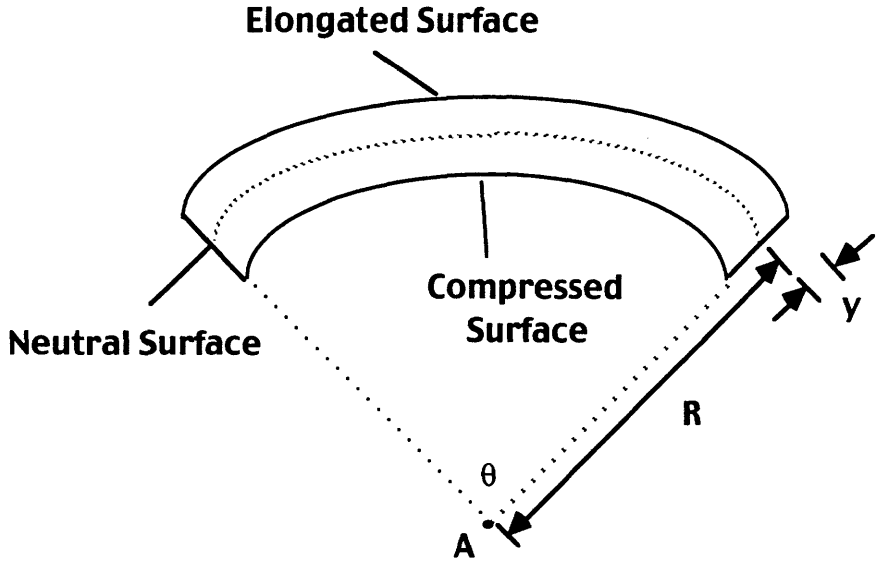

Figure 9. Diagram of Bent Tether

since the length of the neutral surface is the same as the length of the original unbent tether segment the strains at the elongated surface ε_e and the compressed surface ε_c are

$$\varepsilon_e = \frac{l_e - l_n}{l_n} = \frac{(R+y)\theta - R\theta}{R\theta} = \frac{y}{R} \qquad \text{(Equation 19)}$$

and

$$\varepsilon_c = \frac{l_c - l_n}{l_n} = \frac{(R-y)\theta - R\theta}{R\theta} = -\frac{y}{R} \qquad \text{(Equation 20)}$$

From Equation 15 the total measured strain is the difference of the two strains. This allows us to obtain an equation for the radius of curvature of the tether segment

$$\varepsilon_T = \varepsilon_e - \varepsilon_c = \frac{2y}{R} \;\Rightarrow\; R = \frac{2y}{\varepsilon_T} \qquad \text{(Equation 21)}$$

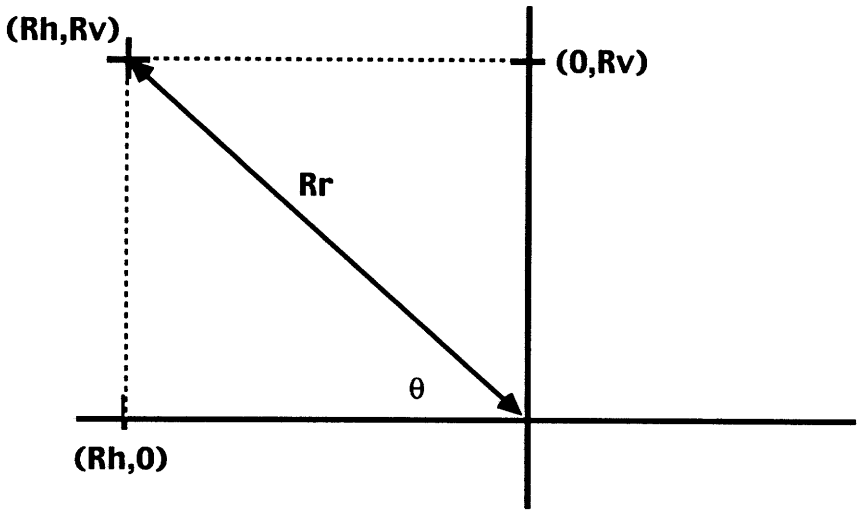

Figure 10. Determining the Resultant Radius of Curvature

As stated above this method is only for determining the bend in the vertical plane. The method will be the same for the bend in the horizontal plane. Figure 10 illustrates the combination of the two radius of curvatures into one resultant radius of curvature. If the vertical radius of curvature R_v and the horizontal radius of curvature R_h are known then the resultant radius of curvature R_r comes simply from the right triangles formed

$$R_r = \sqrt{R_v^2 + R_h^2} \qquad \text{(Equation 22)}$$

and the angle of elevation θ is simply the tangent of the magnitudes of the radii of curvatures, disregarding the effects of the torsional strain on the tether,

$$\theta = \tan\left(\frac{|R_v|}{|R_h|}\right) \qquad \text{(Equation 23)}$$

For this sensor system the distance between the sensor nodes will be the length of the tether segment. The entire segment will be assumed to have the same radius of curvature as measured at the sensor node. Since the relative position of the tether segment is known, it can be attached to the end of the previous segment location. Thus given a particular starting point and the bending strain in the horizontal and vertical directions of each tether segment, the overall position of the tether can be found. It should be noted that this formulation of the tether's position assumes that the tether will not be twisted. The measurement and effects of torsional strain are examined in the next section.

3.1.2 Torsional Measurements [10, 13]

The layout of the sensors to measure the amount of torsional strain is shown in Figure 11. The numbers of the strain gauges, 1 and 2, correspond to their position in the bridge network in Figure 7, omitting 3 and 4. The strain gauges depicted in Figure 11 are rotated by 45° from the horizontal to enable them to measure the torsional strain and not include any effects from the axial or bending strains. However, this orientation will cause the output of each of the strain gauges to be one-half that of an on-axis strain gauge.

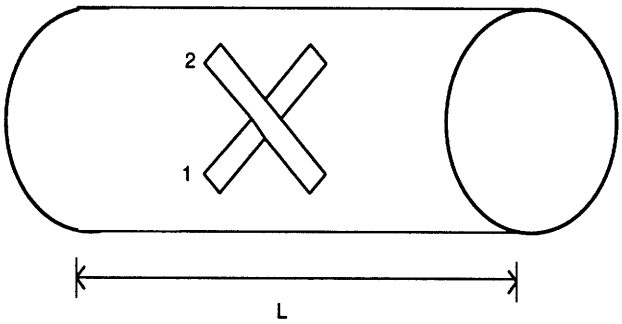

Figure 11. Location of Torsional Sensors

If the left side of the tether is held and the right side is twisted clockwise, Strain gauge 1 (SG1) will be compressed and Strain gauge 2 (SG2) will be elongated. This will cause the resistance of SG1 to increase and the resistance of SG2 to decrease. Therefore, the value of Vout will decrease. If the right side of the tether is twisted counter-clockwise, the value of Vout will increase.

This arrangement of sensors compensates for both axial strains and bending strains. If the segment of tether is either pulled or bent, the resistance of the strain gauges will change by the same amount and Vout will remain unchanged.

A twisted tether segment is illustrated in Figure 12. The torsional strain measured by the sensor arrangement in Figure 11 is defined as the angle of

deformation BAB' in radians, or angle ϕ. The angle BOB' is the angle of twist θ of the length of AB. The angle of deformation can be described by the equation

$$\tan\phi = \frac{BB'}{AB} = \frac{R\theta}{L} \qquad \text{(Equation 23)}$$

since $BB' = R\theta$, and $AB =$ length of segment L. Therefore the angle of twist θ is

$$\theta = \frac{L}{R}\tan\phi \qquad \text{(Equation 24)}$$

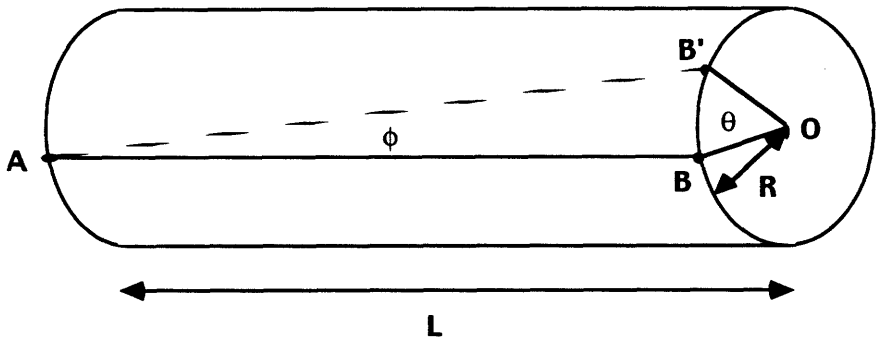

Figure 12. Diagram of Twisted Tether

In Sub-Section 3.1.1 the orientation and position of the tether segment was solely determined by the direction and magnitude of the resultant radius of curvature. The effects of torsional strain were not included. The calculation of the resultant radius of curvature, presented in Sub-Section 3.1.1., will still hold since the two pairs of bend sensing strain gauges are still orthogonal. However, the inclusion of torsional strain will cause an additional rotation of the coordinate system. The angle of rotation for a given tether segment will be the rotation of the previous segment plus the angle of twist θ, determined by Equation 24, for the current tether segment. Therefore both the position and orientation of the tether segment will be dependent upon the previous segment's position and orientation.

It is likely that the spacing of the bend sensor nodes and the torsional sensor nodes will be different. In this case the angle of twist for the bend sensing node will have to be interpolated from the two nearest torsional sensors.

3.2 Expected Results of Strain Gauge Measurements

This section discusses the expected results from using strain gauges to measure the position of an underwater tether, as presented in Section 3.1. Sub-Section 3.2.1 discusses the recommended density of the sensor nodes. Sub-Section 3.2.2 raises issues of the accuracy of the system. Sub-Section 3.2.3 discusses issues of cost.

3.2.1 Density of Sensors

The required density of sensor nodes is very tether specific. Mainly what is needed to determine the density of sensors is the flexibility of the tether and how well the bends and twists are distributed along the tether's length. At this stage of research, some of these values are not well known and this discussion will be somewhat qualitative.

First we will discuss the bend sensor nodes. The one measurement that is required to calculate the needed density of the bend sensors is the maximum rate of change of the radius of curvature. Each tether segment is assumed to have a constant radius of curvature along its length. In order to determine the number of segments needed for a given length, the maximum amount of change in the radius of curvature is needed. This measurement is difficult to quantify and has not yet been made.

An approximation for the density of the bend sensor nodes can be found in another way. The minimum radius of curvature for a tether is a measurement that

is known. For some highly flexible tethers, the minimum radius of curvature is about .25 meters [12]. A coil of tether wrapped at this radius would complete a circle in about 1.6 meters of tether. It would seem reasonable that it would require 3 or 4 arcs of constant curvature to approximate one coil of tether. This would make the distance between the bend sensors about .4-.5 meters. We will use .5 meters throughout the rest of this chapter for ease of computation.

Determining the density of rotational sensors raises a similar problem. The measurement that is needed is the rate of change of the angle of deformation, or rotational strain, as defined in Sub-Section 3.1.2. As an approximation we will assume that the twists in the tether are well distributed along its length. Therefore the rotational strain will be relatively constant along the tether.

In order to obtain an acceptable level of accuracy, it would seem reasonable to find the rotational strain every 1-2 meters. For the calculations in the rest of this chapter, the spacing between the rotational sensor nodes will be assumed to be 1 meter.

3.2.2 Accuracy of Sensors

There are a number of sources of error that may arise in this measurement system. Some sources of error are found in almost any strain gauge measurement. These include misalignment of the gauges, voltage drops in the regulating voltage due to long lead wires, changes in temperature, and the tolerances for certain properties of the strain gauges.

The tolerances of the strain gauges will come into effect if the exact values are not experimentally measured and taken into consideration during the sensor system's operation. The two main measurements of a strain gauge are its nominal resistance and its gauge factor. The nominal resistance is the resistance of the

strain gauge when it is not under any strain. The gauge factor is the proportionality factor between the strain and the change of resistance for a given gauge. Changes in both of these values can directly affect the accuracy of the output voltage.

If the values of each gauge is measured individually and taken into consideration when measuring the strain in the tether, the variances between strain gauges will be insignificant. However if the gauge factor and the nominal resistance of the strain gauge are not measured and are assumed to be the quoted value, significant error may arise.

The tolerance for the gauge factor of a strain gauge, and therefore the error in the output voltage, is ±1% [10]. The tolerance for the nominal resistance is under ±.4% [10]. This tolerance could lead to a significant amount of error in the output signal, dependent upon its size. The worst case would be to have one resistance be 1.004 the quoted value and the other resistance be .996 the quoted value. If the regulated voltage was 10 V, the differences in resistance would lead to a change in the output voltage by 2 mV. Though this may seem quite small, it could be a large percentage of some smaller signals.

Temperature changes can also have an effect on the operation of the strain gauges. The representation of the apparent strain as a function of temperature is called the temperature characteristic. For typical strain gauges, this measurement ranges from about $1x10^{-5}$ to $7x10^{-5}$ (1/°C) [10]. This means that if the temperature is only known within ±100° C, the error of the output signal will be within ±1%. If a guess can be made within ±10° C, the error will be within ±.1%.

If further decreases are needed some temperature circuits could be constructed to determine the temperature within a few degrees (°C). Then the only error would arise from the tolerance of the temperature characteristic, which is about $1x10^{-6}$ [10]. This would correspond to an error well within .01%.

If the tether is very long, then the resistance of the lead wires connecting the strain gauges to the regulated DC voltage could lead to a significant drop in the voltage across the strain gauges. The amount of the drop can be calculated and be accounted for in the operation of the sensor system since the resistances of the wire and the sensors are readily available. The size of the drop can be minimized by either using very thick wire with low resistance or using higher resistance strain gauges. The use of local voltage regulation at each node could also alleviate this problem.

Misalignment of the strain gauges is also a large source of error. If both sensors in a pair are misaligned by only 1 or 2 degrees, the error in the output signal could be a few percent [14]. Since there is no way of knowing how much a sensor is misaligned once the system is constructed, this error cannot be solved and accounted for. Careful application of the strain gauges and the use of larger strain gauges are the best strategies to minimize this source of error.

3.2.3 Cost of Sensors

The cost of this sensors system is divided into the following three parts: the cost per sensor node, the cost of the hardware at the computer terminal, and the cost of constructing the sensor system. The cost per sensor node is the cost of the strain gauges plus the communication ICs mentioned in Section 3.1. Each strain gauge costs around 5 dollars [10]. The ICs for each node would also be around 5 dollars [11]. Given that the suggested spacings of the bend and torsional sensors are .5 meters and 1 meter, respectively, and that there are two strain gauges per node, the total additional cost per meter is around sixty-five (65) dollars. For reference, the cost of most tethers are around thirty (30) dollars per meter [12].

The cost of the hardware will include the serial communication board mentioned in Section 3.1, which is a few hundred dollars, and a computer to determine and display the tether's position using the strain gauge measurements. The biggest expense of the measurement system may be in its construction. Since the placement of the strain gauges need to be very exact, it may require custom design and construction. The relatively high costs and the difficulty to manufacture suggests that the current design of the sensor system will only be used for experimental purposes. Many changes will be needed before this could be available commercially.

3.3 Alternative Technologies

There are several other technologies that may lead to improvements in the current system. Some preliminary research has been conducted in these areas but, more extensive studies are needed to understand the feasibility of them all.

3.3.1 Fiber Optics

Fiber optics is one possible alternative. Using a fiber optic cable as a transmission line, it may be possible to measure the bend of the cable by examining the reflections of an optical pulse sent down the line. Placing fiber optic sensors along the cable may cost less since there would be fewer parts to add to the tether. The main concern with fiber optics is that this approach may require a separate line for each sensor. However, there has been some research in methods of communicating with many fiber optical sensors on one line [15].

3.3.2 Magnetic Sensors

The application of magnetic sensors should also be examined. In the

current design, the orientation of each tether segment is found by a relative measurement of the angle of twist in the cable. Using the earth's magnetic field, magnetic sensors can determine the direction of magnetic north. Combining this information with one other measurement, such as the direction of the earth's gravity, the exact orientation of an object could be determined. Therefore the error in this measurement would be based only on the accuracy of the individual sensors and not on all of the previous orientation sensors. Honeywell, Inc., currently makes some integrated circuits (ICs) that will determine the orientation of an object. There are concerns of cost and size. It is doubtful that a number of ICs will fit on the limited space of an underwater tether and be cheaper than a strain gauge node.

3.3.3 Strain Gauge Rosettes

Another option, though not really a different technology, would be to use a particular arrangement of strain gauges, called a rosette. Rosettes are usually used when the axis of strain is not known. In this case, one rosette could be used to measure both the bend and torsional strains in the tether. If the density of the bend sensors is approximately the same as the density of torsional sensors then it may be better to use a single rosette as opposed to two types of strain gauge orientations. However, if the spacings of the bend and rotational sensors are quite different it would probably cost more to use rosettes since they are much more expensive than normal strain gauges.

3.4 Future Research

There are many areas of future research related to the work presented in this chapter. The eventual goal of this all of this research would be to create a

working sensor system that is reasonably priced and durable. The first step towards that goal would be to investigate the alternative technologies presented in Section 3.3.

Beyond examining new technologies, another area of research would be to obtain a better understanding of the required densities of the relative sensors and how the errors of each segment propagate along the tether. This process would probably need to be done both in experimentation and analysis. As mentioned in Sub-Section 3.2.1 there are some measurements that should be made in order to accurately determine the accuracy given a particular density of sensors, namely the rate of change of the radius of curvature. During this process, it would also be important to examine the possibility of combining the sensor system with a tether model. As mentioned in the introduction, this combination could greatly decrease the system's cost.

Before building a large scale production of the sensor system, the next step would be to build a sensor system for a short piece of tether. The lessons learned in this phase, especially in the construction of the sensor system, are necessary before any final product can be designed. In addition, many tests can be taken on this smaller prototype, such as accuracy and durability.

The final step, if deemed possible by the previous research would be to build a large scale test of the sensor system. Even if this system is not practical enough to be sold commercially, tests on the actual behavior of the underwater tether would be valuable in evaluating and designing physical models of the tether.

4.0 Conclusions

Solving the problem of tether entanglement in underwater remotely operated vehicles is a very complex problem. This thesis presents two attempts at trying to determine the position of the tether. One attempt is through tether modeling. Previous efforts in this area tried to model as many different aspects of the tether's behavior as possible. However, these models are not able to include the higher order effects of bending biases and creep. Essentially this limits the use of using only tether models to simulators and training tools.

Chapter 2 discusses the formulation of a simple tether model that can easily be placed into a virtual reality simulator. For this purpose, the model's speed of computation is more important than the absolute accuracy. The catenary assumed-equation model is a good trade off between computation time and accuracy. It can be computed very quickly and in certain conditions this model is very close to the real solution.

The other attempt to determine the position of an underwater tether is through measuring it directly. Chapter 3 presents a general design for a possible sensor system using strain gauges. Though further research is needed to actually construct the sensor system, this thesis examines the feasibility of this system and some of the expected problems that may arise. The idea of combining tether modeling and sensor measurements has only been mentioned and still requires further research.

Appendix A Derivation of the Flow Catenary [8]

This derivation will show that the equilibrium shape of a inextensible and neutrally buoyant cable immersed in water with a uniform velocity V is in fact a catenary, $f(x) = a\cosh(x/a)$. Figures A1 and A2 below show the coordinate system and the symbol definitions with the following equilibrium equations:

$$(Tx')' + F_x = 0 \qquad \text{(Equation A1)}$$

$$(Ty')' + F_y = 0 \qquad \text{(Equation A2)}$$

subject to

$$(x')^2 + (y')^2 = 1 \qquad \text{(Equation A3)}$$

where T is the tension in the cable and F_x and F_y are the normal drag forces per unit length of tether due to the current.

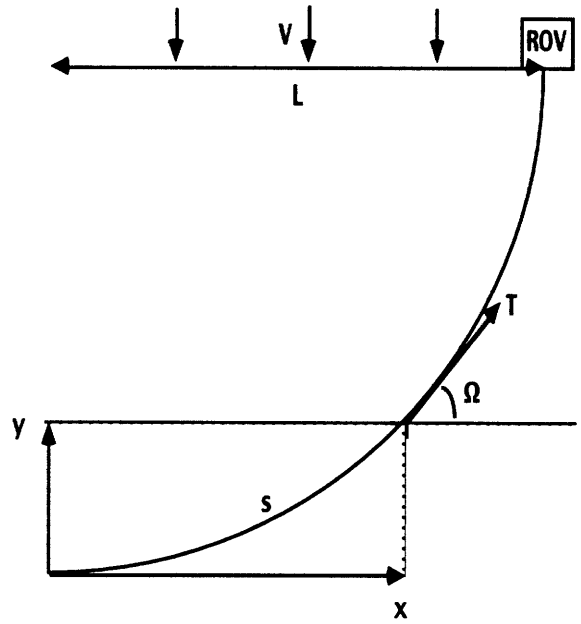

Figure A1. Tether diagram

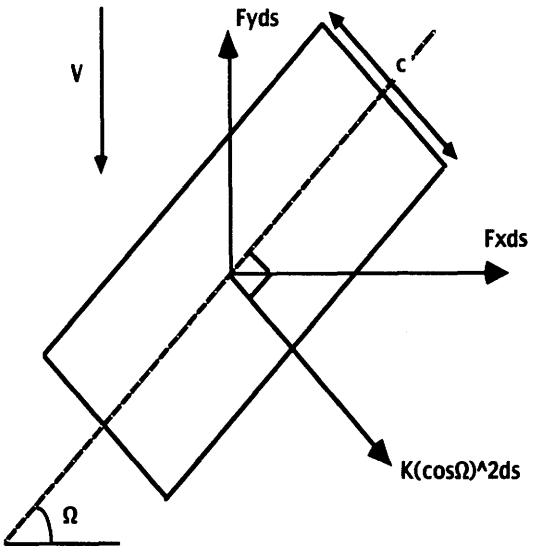

Figure A2. Forces acting on Tether element of length ds

If the fluid density is ρ, the diameter of the chain is c (where c is assumed constant), and C_D is the normal flow coefficient of the cable, then according to the cross-flow principle

$$F_x = \tfrac{1}{2}\rho c C_D V_n^2 \sin\Omega \qquad \text{(Equation A4)}$$

and

$$F_y = -\tfrac{1}{2}\rho c C_D V_n^2 \cos\Omega \qquad \text{(Equation A5)}$$

where F_x and F_y are the forces per unit length of cable in the x and y directions and Ω is the local angle at a given length s. Essentially, the cross-flow principle assumes that the force component along the axis of the chain is only due to skin friction. If the diameter of the chain is fairly uniform along the length then this tangential force component can be neglected and the resultant force is entirely defined by the current normal to the chain. This principle would clearly break down if the variation of c with s were 'strong.' Indeed, while there are many other structures on this principle, it has found wide application and will be adhered to here for simplicity. Since $V_n = V\cos\Omega$, the above equations become

$$F_x = \tfrac{1}{2}\rho V^2 c C_D \cos^2\Omega \sin\Omega \qquad \text{(Equation A6)}$$

and

$$F_y = -\tfrac{1}{2}\rho V^2 c C_D \cos^3\Omega \qquad \text{(Equation A7)}$$

Clearly, $\cos\Omega = x'$ and $\sin\Omega = y'$. Writing $K = (1/2)\rho V^2 c C_D$, the equations of equilibrium become

$$(Tx')' + K(x')^2 y' = 0 \qquad \text{(Equation A8)}$$

and

$$(Ty')' - K(x')^3 = 0 \qquad \text{(Equation A9)}$$

Pulling out the differentiation of the first terms of the equations leaves

$$Tx'' + T'x' + K(x')^2 y' = 0 \qquad \text{(Equation A10)}$$

and

$$Ty'' + T'y' - K(x')^3 = 0 \qquad \text{(Equation A11)}$$

Multiplying (A10) by x' and (A11) by y' and adding it is seen that

$$T' + T(x'x'' + y'y'') = 0 \qquad \text{(Equation A12)}$$

and noting that $x'x'' + y'y'' = 0$,on differentiation of (A3), it follows that

$$T' = 0 \Rightarrow T = \text{constant.} \qquad \text{(Equation A13)}$$

This is not a surprising result since the cross-flow principle is based upon the assumption of zero force along the chain. Again, multiplication of (A10) by y' and (A11) by x' followed by subtraction yields

$$T(x'' y' - y'' x') + K(x')^2 = 0 \qquad \text{(Equation A14)}$$

or

$$T(y'/x')' = K \Rightarrow \left(\frac{dy}{dx}\right)' = \frac{K}{T} = \text{constant.} \qquad \text{(Equation A15)}$$

That is

$$\frac{d}{dx}\left(\frac{dy}{dx}\right) = \frac{K}{T}\frac{ds}{dx} = \frac{K}{T}\sqrt{1+\left(\frac{dy}{dx}\right)^2} \qquad \text{(Equation A16)}$$

which on integration yields

$$\frac{dy}{dx} = \sinh\left(\frac{K}{T}x\right) + C \qquad \text{(Equation A17)}$$

where $C = 0$ since $(dy/dx) = 0$ at $x = 0$. A further integration using $y = 0$ at $x = 0$ yields

$$y = \frac{T}{K}\left[\cosh\left(\frac{K}{T}x\right) - 1\right] \qquad \text{(Equation A18)}$$

Surprisingly, therefore, *the equilibrium shape is a simple catenary*. If the length of the chain is S, the tension T may be obtained from the transcendental equation

$$S = \frac{T}{K}\sinh\left(\frac{K}{T}L\right) \qquad \text{(Equation A19)}$$

where L is the x-distance between the two endpoints.

Appendix B Derivation of the Weight Catenary [9]

This derivation will show that the equilibrium shape of a flexible cable hanging from its ends (and supporting no other weight but its own) is a catenary, $f(x) = a\cosh(x/a)$. Figure A3 shows a cable hanging from a horizontal beam. The lowest point of the cable is a $(0,a)$, where a is a constant that will be determined later. The point (x,y) is a point somewhere on the cable, and can be found by the relation $y = f(x)$. It will be shown that $f(x) = a\cosh(x/a)$.

The cable will be assumed to have a uniform density μ. For instance, the cable could weigh μ Newtons per meter. If s is the length of cable between points (0, a) and (x,y) then the weight of that potion is μs. This force will act downward on point (x,y) as shown in Figure A3. Since the forces acting on the cable are in equilibrium, the upward force of the tension T must balance this weight force.

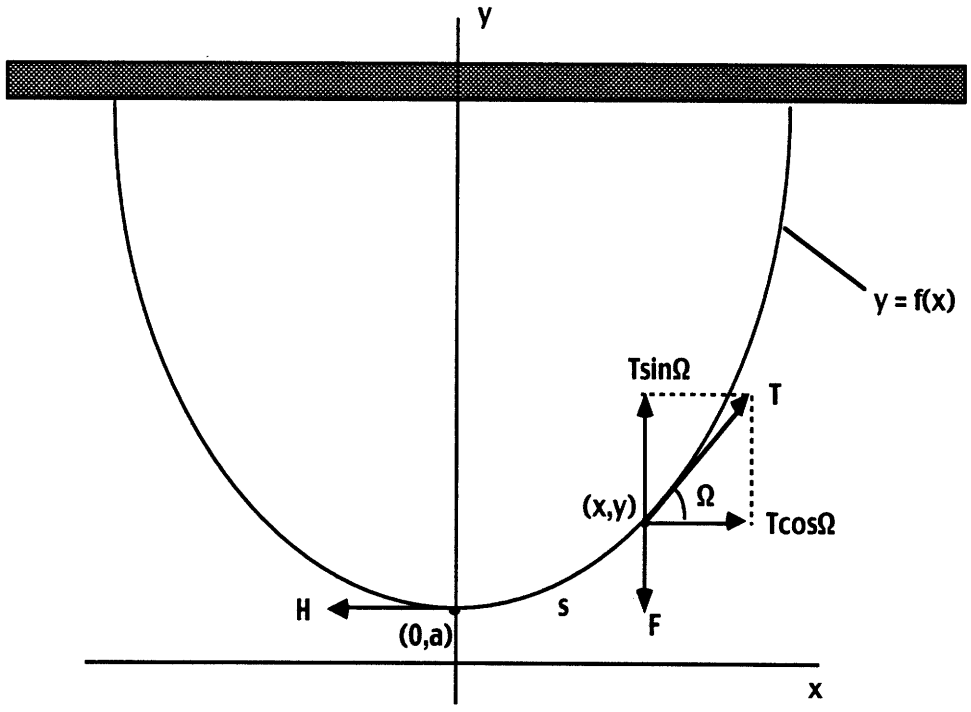

Figure A3. Diagram of a cable hanging under its own weight

The tension T at (x,y) has horizontal and vertical components $T\cos\Omega$ and $T\sin\Omega$, respectively, whereas the tension H at $(0,a)$ is entirely horizontal. The upward force balancing F is therefore $T\sin\Omega$, while the horizontal forces H and $T\cos\Omega$ must cancel each other's effect. In other words, $F = T\sin\Omega$ and $H = T\cos\Omega$. Since T is unknown, we will try to eliminate it by using the slope m at (x,y)

$$m = \tan\Omega = \frac{\sin\Omega}{\cos\Omega} = \frac{F/T}{H/T} = \frac{F}{H} = \left(\frac{\mu}{H}\right)s \qquad \text{(Equation A20)}$$

Let $k = \mu / H$(constant because the density μ and the tension H at the lowest point of the cable are constant). Then $m = ks$. Since $m = dy/dx$, this is a differential equation involving out unknown function $y = f(x)$, which on integration yields

$$\frac{dy}{dx} = \sinh(kx) + C \qquad \text{(Equation A21)}$$

where $C = 0$ since $m = dy/dx = 0$ at $x = 0$. Hence, a further integration using $y = a$ at $x = 0$ yields

$$y = \frac{1}{k}\cosh(kx) + \left(a - \frac{1}{k}\right) \qquad \text{(Equation A22)}$$

conveniently choosing $a = 1/k$ reduces the equation to

$$y = a\cosh(x/a) \qquad \text{(Equation A23)}$$

which is the equation that we were trying to derive, *the catenary*. An interesting problem is now to solve for the tension T at a given point (x,y). From Equation A20 and A21 we note that

$$ks = \sinh(kx) \qquad \text{(Equation A24)}$$

differentiating both sides with respect to x and noting that $\cos\Omega = dx/ds$ leads to

$$\sec\Omega = \cosh(kx) \qquad \text{(Equation A25)}$$

using the relations given in the text above, $H = T\cos\Omega$ and $H = \mu/k$,

$$T = \mu a \cosh\left(\frac{x}{a}\right) = \mu y \qquad \text{(Equation A26)}$$

Thus the tension on the point (x,y) is simply the density μ times the height, or y-value, of the point.

References

[1] F.S. Hover, Simulation of stiff massless tethers. *Ocean Engineering*, to appear.

[2] A. Blieke, Dynamic analysis of single span cables. 1984 O.E. PhD Thesis, MIT, Cambridge, MA.

[3] C.M. Ablow and S. Schecter, Numerical simulation of undersea cable dynamics. *Ocean Eng.* Vol. 10, No. 6, pp 443-457, 1983.

[4] C.T. Howell, Numerical analysis of 2-D nonlinear cable equations with applications to low-tension problems. *Int. J. Offshore and Polar Eng.* Vol. 2, No. 2, pp 110-113, 1992.

[5] M.A. Grosenbaugh, C.T. Howell, and S. Moxnes, Simulating the dynamics of underwater vehicles with low-tension tethers. *Int. J. Offshore and Polar Eng.* Vol. 3, No. 3, pp 213-218, 1993.

[6] N. Dennis, The "two century plus" history of the constant-tension catenary as applied to tall ship sails, paravan and other tows, oil slick catch booms and some buoy moors. *Oceans '95 MTS/IEEE Conference Proceedings.* Oct. 9-12, 1995. San Diego, CA.

[7] N. Dennis, On the formation of funicular curves. *Int. J. Mech. Sci.* Vol. 36, No. 3, pp 183-188, 1994.

[8] A.Simpson and B.Tabarrok, On the equilibrium configuration of a chain subjected to uniform fluid flow in a horizontal plane. *Int. J. Mech. Sci.* Vol. 18, pp 91-94, 1976.

[9] P. Gillett, *Calculus and analytical geometry.* D.C. Heath, Lexington, Massachusetts, 1984.

[10] *The pressure, strain, and force handbook.* Omega Engineering, Inc., Vol. 27, 1991.

[11] *Analog Design Guide.* Maxim Integrated Products, Inc., 13th Edition, 1998.

[12] *Catalog.* Cortland Cable Co., 1998.

[13] J. Hannah and M.J. Hillier, *Applied mechanics.* Longman Scientific & Technical, Essex, England, 1995.

[14] A.L. Window, *Strain gauge technology.* Elsevier Applied Science, New York, 1989.

[15] G.F. Lutes and X.S. Yao, Swept-frequency fiber-optic readout from multiple sensors. *NASA Tech Briefs*, October 1997, p35.